DYNAMIC DEFORMATION AND FAILURE OF NANOWIRES

WUWEI LIANG & MIN ZHOU

School of Mechanical Engineering, Georgia Institute of Technology, Atlanta, GA 30332-0405, U.S.A.

ABSTRACT

MD simulations with an embedded atom method (EAM) potential are carried out to study the dynamic tensile deformation and failure of copper nanowires suspended between tips. The study focuses on the deformation mechanisms and the size and strain rate effects in the tensile deformation of Cu nanowires. The nanowires analyzed are single-crystals with axes in the [001], [010], and [001] directions. The cross-sections of the nanowires are squares with dimensions between 5 and 20 lattice constants (or 1.8~7.2 nm). The length of the specimens is 60 lattice constants (or 21.6 nm). Deformations under constant strain rates between 1.67×10^{5} s^{-1} and 1.67×10^{10} s^{-1} are analyzed. It is found that at low strain rates a well-structured activation of stacking faults and twins on alternating slip planes is the primary deformation mode. The inability of dislocations to travel at speeds higher than the shear wave speed of the material imposes a critical strain rate above which amorphization is observed. The ductility of nanowires does not vary significantly with strain rates when plastic deformation progresses through dislocation motion. A significant dependence of ductility on strain rate is observed when amorphization is the primary deformation mechanism. There is also a clear transition in deformation mechanism as specimen size is changed. Specifically, when cross-sectional dimensions are on the order of 3-8 lattice spacings, a single dislocation is nucleated and moves along a pair of slip planes. At larger cross-sectional sizes (10-20 lattice constants), multiple dislocations are nucleated from the free surface and move into the nanowires as the plastic deformation progresses. Ductility increases with specimen size as a result of enhanced opportunities for dislocation motion at larger sizes.

1. INTRODUCTION

As functional nano-building-blocks, nanowires have a variety of potential applications in many areas such as chemical sensors, nano-electronics, and nano-photonics. Such exciting application potentials have motivated intensive research on nanowires of different materials in recent years. Nanowires are usually assembled between substrates or suspended between tips. At the nanoscale, minute movements of the substrates or tips can cause significant deformation and even failure of nanowires. The movement of the substrates or tips may be due to mechanical loading, thermal expansion or contraction. Hence, it is essential to understand the mechanical behaviors of nanowires in the assembling of nanowires into functional devices. In this study, MD simulations with an embedded atom method (EAM) potential[1, 2] are carried out to study the dynamic tensile deformation and failure of Cu nanowires suspended between two tips. The study concerns the deformation mechanisms and the size and strain rate effects in dynamic tensile loading. The cross-sections of the nanowires are squares with dimensions between 5 and 20 lattice constants (1.8~7.2 nm). The length of the specimens is 60 lattice constants (21.6 nm). Deformations under constant strain rates between 1.67×10^{5} s^{-1} and 1.67×10^{10} s^{-1} are analyzed.

2. COMPUTATIONAL SETUP

The MD simulations carried out concern the simple tension of single crystal Cu nanowires, as illustrated in Fig. 1. The nanowires have free surfaces in the x- and y-directions. The x-, y-, and z-axes are oriented in the [100], [010], and [001] crystalline directions, respectively. Constant velocities of $\pm V_0$ are applied on boundary atoms (red) at the top and bottom ends, thus effecting the loading necessary for the nanowire to deform at a constant nominal strain rate of $\dot{\varepsilon} = 2V_0 / L$.

The internal atoms simply deform with the boundary atoms. A uniform initial thermomechanical state at a temperature of 300 K and fixed length is obtained through MD calculations with the Nose-Hoover thermostat procedure while the wire length is kept constant. The nanowires are not relaxed to a zero stress state and the beginning of deformation is at stress levels of 0.4-1.6 GPa, depending on the wire size. The calculations are carried out with a time step of 1 fs until fracture occurs.

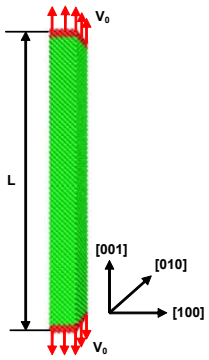

Figure 1: A schematic illustration of the computational model for Cu nanowires

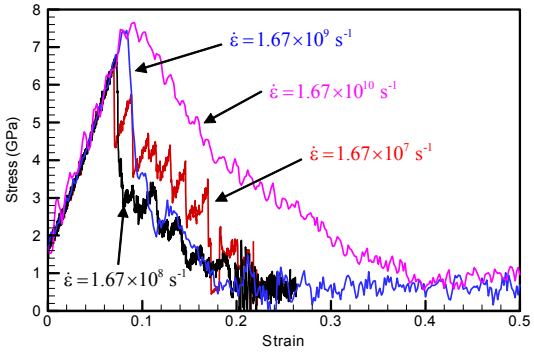

Figure 2: Stress-strain curves of 5×5×60 Cu nanowires at different strain rates

3. DEFORMATION MECHANISMS

Figure 2 shows the stress-strain relations at strain rates between 1.67×10^{7} s^{-1} and 1.67×10^{10} s^{-1}. The cross-sectional size of the wires here is 5×5 lattice constants (1.8×1.8 nm). The nanowire exhibits very different responses at strain rates below 1.67×10^{10} s^{-1} and at strain rates above 1.67×10^{10} s^{-1}. Specifically, the curves at strain rates below 1.67×10^{10} s^{-1} show precipitous drops in stress after yielding. These sharp drops are associated with the initiation of plastic deformation which occurs through dislocation motion along {111} slip planes and formation of stacking faults. In contrast, stress decreases only gradually after the onset of inelastic deformation at strain rates above 1.67×10^{10} s^{-1}. Furthermore, the wire shows a much higher level of ductility than those at the lower strain rates. This change in behavior is due to a transition in deformation mechanism from the formation of stacking faults through dislocation motion to amorphization. This observation of transition in deformation mechanism is consistent with what was reported for metallic wires in the literature[3]. The significantly higher level of ductility can be regarded as a form of superplacticity in nanowires.

3.1. Propagation of Stacking Faults

Unlike the plastic deformation of bulk materials which involves the nucleation, motion and interaction of a large number of dislocations, the plastic deformation of nanowires can involve only a small number or even a single pair of partial dislocations due to the extremely small sizes. The particular number of dislocations seen depends on the size of the nanowires. It is observed that when the lateral wire size is smaller than 5×5 (lattice constants), sequential nucleation and motion of a single pair of partial dislocations is primarily responsible for the plastic deformation at the strain rates lower than 1.67×10^{9} s^{-1}. On the other hand, multiple dislocations are nucleated when the size is larger than 8×8. In this case, the number of dislocations also varies with strain rate. Generally, the number of dislocations is higher at higher strain rates.

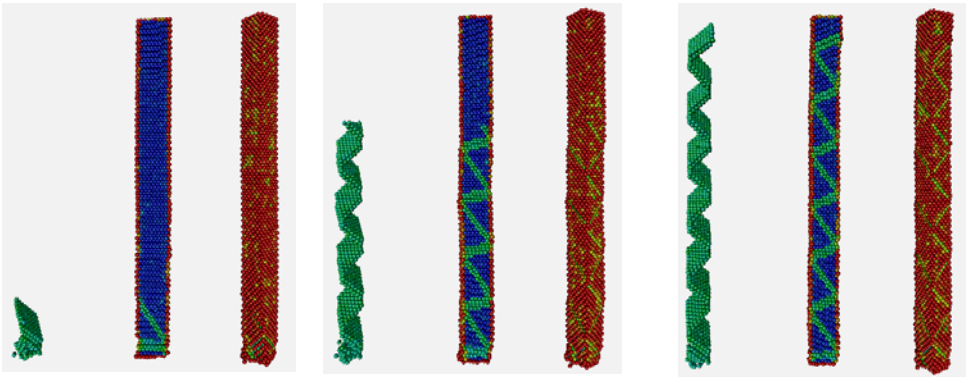

(a) (b) (c)

Figure 3: Propagation of dislocations at a strain rate of $1.67\times10^{8}\ s^{-1}$, (a) $\varepsilon = 4.67\%$, (b) $\varepsilon = 5.33\%$, and (c) $\varepsilon = 6.0\%$. The specimen size is 5×5×60.

When the wire is smaller than 5×5 lattice constants, only a single dislocation is nucleated. The dislocation always nucleates at the corner of one end of the nanowires (see Fig. 3(a)) and glides along {111} slip planes in <112> directions after nucleation. Intrinsic stacking faults are formed behind the partial dislocations, see Fig 3(b, c). The tensile loading along the [001] directions induces higher resolved shear stresses for slip in $<11\bar{2}>$ directions than for slip in $<1\bar{1}0>$ directions on {111} planes. Specifically, the Schmid factor for the $[11\bar{2}]$ direction (0.47) is greater than that for the $[1\bar{1}0]$ direction (0.41). Therefore, the formation of stacking faults through dislocation motion in <112> directions on {111} planes is the preferred action under the loading condition considered. The partial dislocation pair generates a step when it reaches a free surface. This step leads to the nucleation and motion of another dislocation on an alternate {111} slip plane, leading to sequential stacking faults formation on alternating {111} planes, see Fig 3(c).
For the loading condition in Fig. 3, the average speed at which the active front of stacking faults propagates along the wire axis is 355 ms^{-1}. The instantaneous speed oscillates between zero and a maximum on the order of 1,000 ms^{-1}, reflecting the alteration of the propagating front between the two {111} planes. The level of the speed observed here constitutes significant fractions of the stress wave speeds in Cu. In particular, note that the stress wave speed in the <001> direction of single crystal copper is 2,092 ms^{-1} for uniaxial stress and 4,198 ms^{-1} for uniaxial strain. We will discuss in section 4.1 the critical role played by the dislocation speed in the transition of deformation mechanisms. In particular, we will show that amorphization occurs as a result of the fact that the dislocation speed can not exceed the shear wave speed in the material.

3.2. Local Structural Transformation and Twinning

In bulk materials, twinning tends to occur in BCC and HCP crystals, since they have fewer slip systems compared with FCC crystals. In the FCC nanowires analyzed here, the stress-induced slip on different combinations of slip planes can also lead to local HCP structures or twins in addition to stacking faults. Specifically, stacking faults, twins, and local FCC→HCP transformation can all be produced by the same type of shearing operations on the {111} planes in $<2\bar{1}\bar{1}>/6$ directions. The shear operation is completed through the motion of partial dislocations, as discussed previously. A stacking fault is formed through the shear operation in the $[\bar{2}11]/6$ direction when

only two {111}-type atomic planes are involved, see Fig. 4(a). An additional shearing operation between a pair of neighboring {111}-type planes in the $[2\bar{1}\bar{1}]/6$ direction generates a local stacking sequence of ABABAB…, leading to the formation of a local HCP structure, see Fig. 4(b). This HCP structure has a higher Gibbs free energy than the corresponding equilibrium FCC structure and is thermodynamically unstable under the conditions discussed. This instability causes another shearing operation on another pair of {111}-type planes, restoring the local structure to FCC. The newly formed FCC structure is a mirror image of the un-rotated portions of the original wire, forming a pair of twins, see Fig. 4(c). Experimental measurements and theoretical calculations indicate that $\gamma_I \sim 2\gamma_T \sim 2\gamma_H$, with γ_I and γ_T representing the energies of intrinsic and twin faults, respectively, and γ_H representing the FCC→HCP transformation energy per layer. Consequently, stacking faults tends to be observed at early stages of the plastic deformation when the stress and energy level are high. In contrast, local FCC→HCP transformation and twinning occur at relatively lower stress levels after stacking faults are formed in the wire.

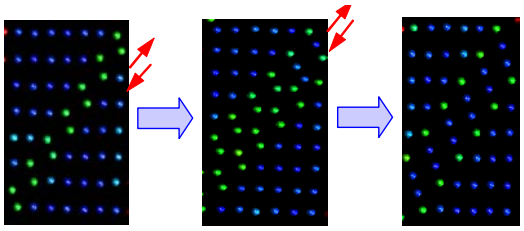

(a) (b) (c)

Figure 4: Transition of defects: stacking faults → local HCP structure → twins

3.3. Nucleation of Multiple Dislocations

As the wire size increases, dislocation mobility is enhanced. Specifically, multiple dislocations can be nucleated when the wire size is larger than 8×8. Dislocations are usually nucleated from free surfaces which act as important dislocation sources in defect-free single crystal nanowires. Once nucleated, dislocations start to move from surfaces to the interior of the nanowires along different {111} slip planes. This process results in networks of stacking faults, local HCP structure and twins. The multiple dislocation generation and interaction cause the stress decreases after the onset of yielding in larger wires to be more gradual than the stress decreases in small wires. The enhanced opportunities for dislocation nucleation and motion also lead to higher levels of ductility for thicker wires.

3.4. Amorphization

The nanowires exhibit a significantly different tensile behavior when the strain rate reaches approximately $1.67\times10^{10}\ s^{-1}$. At such high strain rates, the plastic deformation no longer progresses through the propagation of stacking faults, local FCC→HCP transformation, or twinning. Instead, the nanowire goes through a phase transformation from ordered crystalline structure to an amorphous state. The amorphization always starts in the middle of the nanowire and expands toward the ends as the deformation progresses. Nanowires exhibit significantly higher levels of ductility when amorphization occurs. Calculations show that amorphization is both size and strain rate dependent, as we will discuss later.

4. SIZE AND STRAIN RATE EFFECTS

4.1. Critical Strain Rate for Amorphization

As discussed above, when the lateral dimension of the nanowire is smaller than 5×5 lattice constants the plastic deformation of the nanowire involves the nucleation and movement of a single partial dislocation. A simple analysis can be carried out to relate the average strain rate to dislocation speed and wire size. If the deformation is produced by the dislocation movement only, then the strain rate can be expressed as

$$\dot{\varepsilon} = \frac{av}{3\sqrt{6}Lr}, \tag{1}$$

where a is the lattice constant, v is dislocation velocity, L and r are the length and lateral dimension of the nanowire, respectively. Equation (1) can be extended to account for situations with multiple dislocations in the wire (when the wire size is larger than 8×8 lattice spacings). Specifically, for wires with n dislocations

$$\dot{\varepsilon} = \frac{na\bar{v}}{3\sqrt{6}Lr}, \tag{2}$$

where $\bar{v}$ is the average velocity of all dislocations.

We can see from Eq. (1) that the dislocation velocity increases with the strain rate. Since the dislocation velocity can not exceed the shear wave speed v_s of the material, there exists a maximum strain rate that can be accommodated by the motion of dislocations. This limiting strain rate is given by

$$\dot{\varepsilon}_c = \frac{av_s}{3\sqrt{6}Lr}. \tag{3}$$

Strain rates higher than $\dot{\varepsilon}_c$ can not be accommodated by the motion of dislocations only and must entail other deformation mechanisms such as amorphization. For a given material, this critical strain rate is lower for larger wires. For a copper nanowire of size 5×5×60, $a = 3.615$ Å, $L = 60a$, $r = 5a$, and $v_s = 2291$ ms^{-1}, yielding a critical strain rate of $\dot{\varepsilon}_c$=2.87×10^9 s^{-1}. This calculated critical strain rate agrees reasonably well with our simulation results. Indeed, calculations show that the propagation of dislocations is primarily responsible for the plastic deformation when the strain rate is lower than 2.87×10^9 s^{-1}. On the other hand, amorphization is the dominant mechanism when the strain rate is higher than 2.87×10^9 s^{-1}.

4.2. Rate and Size Dependence of Yield Stress

The critical stress for the onset of plastic deformation (yield strength) is the stress required to create and move dislocations and other structural defects. For bulk materials, the stress dependence of dislocation velocity has been fitted into different types of equations, some empirical, some with theoretical backing. In general, dislocation velocity increases with increasing resolved stress on the slip system. The same trend has been observed in nanowires as well. The relationship between dislocation velocity and applied stress can be summarized as

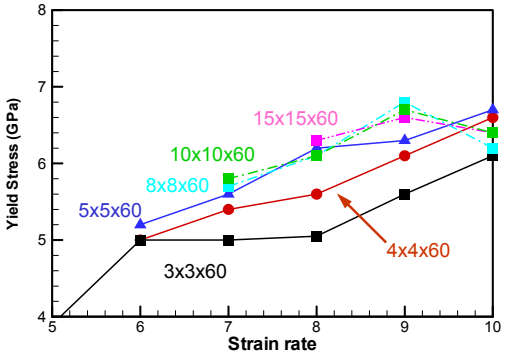

Figure 5: The variation of yield stress with strain rate and wire size

$$v_{disl} \propto \sigma \,. \tag{4}$$

Equations (1) and (4) show that

$$\sigma \propto \frac{Lr\dot{\varepsilon}}{na} \,. \tag{5}$$

Figure 5 shows the calculated the yield stress as a function of strain rate. For the same strain rate, the yield stress increases with the wire size when the wire size is smaller than 5×5 lattice spacings. When the wire size is above than 8×8 lattice constants, the yield stress is essentially independent of wire size. This may be because the number of nucleated dislocations increases proportionally with the wires size.

5. CONCLUSION

MD simulations of the tensile deformation of single crystal Cu nanowires are performed using an embedded atom method. The effects of strain rate and size sale on behavior are studied. At low strain rates, dislocation nucleation and motion on {111}-type slip planes are the primary deformation mode. For wires with lateral dimensions smaller than 8×8 lattice spacings, a well-structured activation of stacking faults and twins on alternating slip planes is the primary deformation mode. The inability of dislocations to travel at speeds higher than the shear wave speed of the material imposes a critical strain rate above which amorphization is observed. There is also a clear transition in deformation mechanism as specimen size is changed. Specifically, when the cross-sectional dimensions are on the order of only a few lattice spacings, a single dislocation is nucleated and moves along a pair of slip planes. At larger cross-sectional sizes (10-20 lattice constants), multiple dislocations are nucleated from the free surface of the nanowires and move into the nanowires as the plastic deformation progresses. Ductility is found to increase with specimen size as a result of enhanced opportunities for dislocation motion at larger sizes. For the same reason, the yield stress is found to be lower for larger wire sizes.

ACKNOWLEDGMENTS

Support from NASA Langley Research Center is gratefully acknowledged. Computations are carried out on the supercomputers at the NAVO and ERDC MSRCs. We would like to thank S. Plimpton for sharing his MD code. The images of deformation in this paper are created with the graphics package Visual Molecular Dynamics (VMD)[4].

REFERENCES

1. Daw, M. S. and Baskes, M. I.,"Embedded-atom method: Derivation and application to impurities, surfaces, and other defects in metals", *Physical Review B (Condensed Matter)*, 1984. Vol. 29, No. 12: pp. 6443-6453.

2. Daw, M. S., Foiles, S. M., and Baskes, M. I.,"The embedded-atom method: a review of theory and applications", *Material Science Reports*, 1993. Vol. 9, No. 7-8: pp. 251-310.

3. Ikeda, H., Qi, Y., Cagin, T., Samwer, K., Johnson, W. L., and Goddard, W. A. I.,"Strain rate induced amorphization in metallic nanowires", *Physical Review letters*, 1999. Vol. 82, No. 14: pp. 2900-2903.

4. Humphrey, W., Dalke, A., and Schulten, K.,"VMD - Visual Molecular Dynamics", *J. Molec. Graphics*, 1996. Vol. 14, No. 1: pp. 33-38.